


SCIENTIFIC REPORTS



OPEN

Thermoelectric and phonon transport properties of two-dimensional IV–VI compounds

Aamir Shafique & Young-Han Shin

We explore the thermoelectric and phonon transport properties of two-dimensional monochalcogenides (SnSe, SnS, GeSe, and GeS) using density functional theory combined with Boltzmann transport theory. We studied the electronic structures, Seebeck coefficients, electrical conductivities, lattice thermal conductivities, and figures of merit of these two-dimensional materials, which showed that the thermoelectric performance of monolayer of these compounds is improved in comparison compared to their bulk phases. High figures of merit (ZT) are predicted for SnSe ($ZT = 2.63, 2.46$), SnS ($ZT = 1.75, 1.88$), GeSe ($ZT = 1.99, 1.73$), and GeS ($ZT = 1.85, 1.29$) at 700 K along armchair and zigzag directions, respectively. Phonon dispersion calculations confirm the dynamical stability of these compounds. The calculated lattice thermal conductivities are low while the electrical conductivities and Seebeck coefficients are high. Thus, the properties of the monolayers show high potential toward thermoelectric applications.

Renewable energy is a very important field due to the insufficiency of natural energy source and global warming¹. One of the best renewable energy sources is waste heat, which can be converted into electricity via the Seebeck effect^{2,3}. The performance of thermoelectric materials is measured by a dimensionless quantity ZT called the figure of merit^{4,5}:

$$ZT = \frac{\sigma S^2}{\kappa} T \quad (1)$$

where σ , S , κ , and T are electrical conductivity, Seebeck coefficient, thermal conductivity, and temperature, respectively. The lattice thermal conductivity κ_l and the electronic thermal conductivity κ_e are included in the thermal conductivity κ in eq. 1. A large Seebeck coefficient, large electrical conductivity, and low thermal conductivity are needed for high thermoelectric performance, but a low amount of charge carrier is required to improve the Seebeck coefficient, which reduces the electrical conductivity⁶.

Improving ZT has been a big challenge, and different approaches have been used. Semiconductors composed of heavy elements such as Zn_4Sb_3 , PbTe and BiSb have been used to reduce the thermal conductivity^{7–9}. Point defects ($\text{R}_{1-y}\text{Fe}_{4-x}\text{Co}_x\text{Sb}_{12}$ and $\text{Ce}_y\text{Fe}_x\text{Co}_{4-x}\text{Sb}_{12}$) have been produced to decrease the lattice thermal conductivity and the optimized electrical conductivity^{10,11}. Some bulk complex materials also show very good thermoelectric performance such as filled skutterudites ($\text{La}_{0.9}\text{Fe}_3\text{CoSb}_{12}$), half-Heusler alloys ($\text{ZrCoSn}_x\text{Sb}_{1-x}$), and clathrates ($\text{Sr}_8\text{Ga}_{16}\text{Ge}_{30}$) because of their low thermal conductivity and high periodicity in the crystal structure^{12–16}. Zhao *et al.* recently reported that bulk SnSe is a very good thermoelectric material with a ZT of 2.6 at 973 K¹⁷. It was theoretically predicted that bulk SnS, GeSe, and GeS would also show very good thermoelectric performance¹⁸.

One of the efficient methods to increase ZT is reducing the dimensionality of the material, which increases the Seebeck coefficient due to the increased density of states near the Fermi level^{19–21}. It is reported that the reduction in dimensionality enhances the energy storage and conversion^{22,23}, the ZT of bulk Bi_2Te_3 is improved 13 times by converting into the quantum well. Fei *et al.* and Cheng *et al.* reported that a bismuth monolayer and phosphorene showed very promising thermoelectric properties^{24,25}.

We studied two-dimensional SnSe, SnS, GeSe, and GeS materials for thermoelectric applications. Monolayers of these materials have already been experimentally synthesized, and they have band gaps less than 2 eV^{26–29}. They have been recently reported to have low lattice thermal conductivity as well³⁰, which is a requirement for efficient thermoelectric materials. Group IV–VI compounds in bulk form have very good thermoelectric efficiency and a

Department of Physics, University of Ulsan, Ulsan, 44610, Republic of Korea. Correspondence and requests for materials should be addressed to Y.-H.S. (email: hopenpop@ulsan.ac.kr)

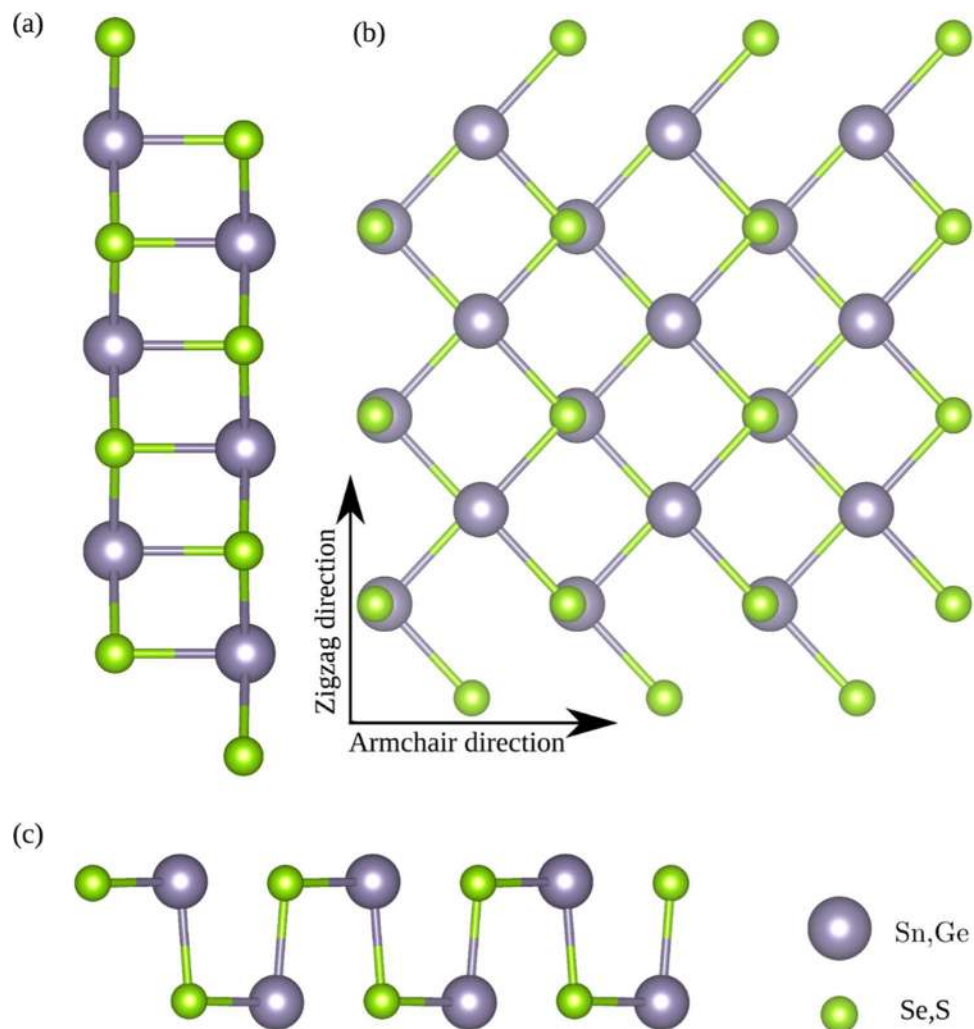


Figure 1. Crystal structure of two-dimensional monochalcogenides SnSe, SnS, GeSe, and GeS. (a) Side view perpendicular to the zigzag direction, (b) top view, (c) side view perpendicular to the armchair direction.

| Composition | Lattice parameter (Å) | | Band gap (eV) | |
|-------------|-----------------------|-------------|---------------|-------------|
| | Monolayer | | Monolayer | Bulk |
| | <i>a</i> | <i>b</i> | GGA | GGA |
| SnSe | 4.46 (4.41) | 4.29 (4.27) | 0.99 (1.00) | 0.65 (0.69) |
| SnS | 4.31 (4.26) | 4.07 (4.06) | 1.42 (1.52) | 0.86 (0.91) |
| GeSe | 4.41 (4.38) | 3.99 (3.95) | 1.16 (1.22) | 0.83 (0.87) |
| GeS | 4.48 (4.43) | 3.70 (3.67) | 1.71 (1.70) | 1.18 (1.25) |

Table 1. Calculated lattice parameters and band gaps of SnSe, SnS, GeSe, and GeS. The values in the parentheses are from the refs 18 and 34.

simple orthorhombic SnSe crystal was reported to have outstanding thermoelectricity^{17,31,32}. It was recently discovered that even a monolayer of SnSe shows optimal thermoelectric properties³³, which motivated us to study the thermoelectric properties of monolayer IV–VI compounds SnSe, SnS, GeSe, and GeS.

Results and Discussions

Bulk SnSe, SnS, GeSe, and GeS have an orthorhombic crystal structure with the space group $Pnma(62)$, while their monolayer analogs have the space group $Pmn2_1(31)$ (see Fig. 1). The structures are optimized with a large vacuum space of 15 Å in the z -direction until the forces on each atom become zero. The optimized lattice parameters are given in Table 1, and they are in good agreement with previous reports^{34,35}.

Electronic structures are very important for understanding the thermoelectric behavior of materials. The band gaps of SnSe, SnS, GeSe, and GeS are calculated using the exchange-correlation functional within a generalized

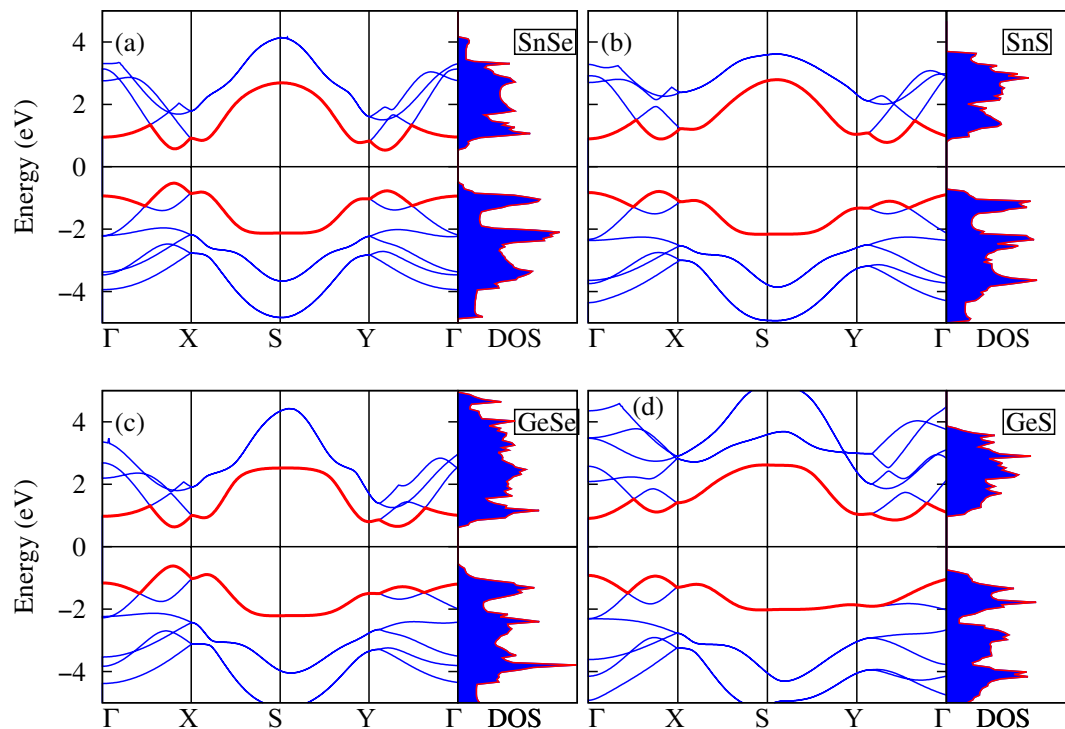


Figure 2. Band structures along the high-symmetry k -points Γ , X, S, and Y and density of states of (a) SnSe, (b) SnS, (c) GeSe, and (d) GeS.

gradient approximation (GGA), as shown in Table 1. The GGA functional calculations show indirect band gaps for SnSe, SnS, and GeS and a direct band gap for GeSe, as shown in Fig. 2. Density of states (DOS) of the SnS and GeS monolayers has sharp peaks near conduction band minima and valence band maxima as shown in Fig. 2(b,d), which may enhance the Seebeck coefficient. All these monolayers have band gaps less than 2 eV, which suggests that they can be used as thermoelectric materials. It is very difficult to get the optimal value of the ZT for wide band gap materials because heavy doping is required.

The carrier mobility (μ) of the group IV–VI monolayers is calculated in order to get relaxation time (τ). Our method to calculate the mobility is based on deformation potential theory used extensively to calculate carrier mobility and relaxation time of two-dimensional materials^{36–39}, the expression to calculate the mobility is given by^{36,39,40}:

$$\mu = \frac{e\hbar^3 C^{2D}}{k_B T m^* m_d E_1^2} \quad (2)$$

where C^{2D} is the two-dimensional elastic constant determined by fitting the energy-strain curve to quadratic polynomial (see Fig. S1), our calculated values for C^{2D} are consistent with previous reported values⁴¹. T represents the temperature, m^* is the effective mass in the transport direction, and m_d is calculated as $m_d = \sqrt{m_x m_y}$. Here m_x and m_y are the effective masses along armchair and zigzag directions. E_1 is the deformation potential constant defined by $E_1 = \partial E_{edge} / \partial \delta$, where E_{edge} is the conduction band minima (CBM) and δ is uniaxial strain. The shift in CBM by applying uniaxial strain is shown in Supplementary Fig. S2. The relaxation time is evaluated from mobility using the following relation:

$$\tau = \frac{m^* \mu}{e} \quad (3)$$

The calculated E_1 , C_{2D} , m^* and temperature-dependent μ and τ are tabulated in Table 2. We found an anisotropic behaviour in mobility and relaxation time for these monolayer. The carrier mobility of SnSe is in a good agreement with ref. 38. The GeS has the highest carrier mobility and relaxation time along the armchair direction among these four monolayer due to the low deformation constant and the low effective mass.

The thermoelectric properties of SnSe, SnS, GeSe, and GeS are calculated using the Boltzmann transport equation for electrons under a constant scattering time. Boltztrap code calculates relaxation-time dependent electrical conductivity (σ/τ) and electronic thermal conductivity (κ_e/τ). Since there is no experimental data available for the electrical conductivity to calculate the exact value of the relaxation time of these monolayers, deformation potential theory is used to predict the temperature-dependent relaxation time for each material as compiled in Table 2. The electrical (σ) and electronic thermal (κ_e) conductivities are plotted as a function of carrier concentration (n) in Fig. 3(a–d) and (e–g) respectively, at 300 K, 500 K, and 700 K along armchair and zigzag directions.

| Composition | Direction | E_1 (eV) | C^{2D} (N/m) | m^* (m_e) | T = 300 K | | T = 500 K | | T = 700 K | |
|-------------|-----------|------------|----------------|-----------------|---|-------------|---|-------------|---|-------------|
| | | | | | μ ($\text{cm}^2 \text{V}^{-1} \text{s}^{-1}$) | τ (fs) | μ ($\text{cm}^2 \text{V}^{-1} \text{s}^{-1}$) | τ (fs) | μ ($\text{cm}^2 \text{V}^{-1} \text{s}^{-1}$) | τ (fs) |
| SnSe | Armchair | 3.32 | 12.46 | 0.15 | 1035.84 | 88.35 | 621.50 | 53.01 | 443.93 | 37.86 |
| | Zigzag | 4.70 | 24.82 | 0.16 | 965.23 | 87.82 | 579.13 | 52.69 | 413.60 | 37.63 |
| SnS | Armchair | 2.78 | 14.08 | 0.24 | 623.54 | 85.10 | 374.13 | 51.06 | 267.23 | 36.47 |
| | Zigzag | 4.27 | 26.05 | 0.28 | 419.10 | 66.73 | 251.48 | 40.04 | 179.63 | 28.60 |
| GeSe | Armchair | 2.49 | 12.11 | 0.27 | 541.24 | 83.10 | 324.74 | 49.86 | 231.96 | 35.61 |
| | Zigzag | 3.91 | 28.35 | 0.30 | 465.01 | 79.33 | 279.01 | 47.59 | 199.29 | 33.99 |
| GeS | Armchair | 2.37 | 13.89 | 0.19 | 1045.40 | 112.95 | 627.24 | 67.77 | 448.03 | 48.40 |
| | Zigzag | 3.70 | 33.40 | 0.37 | 529.57 | 111.43 | 317.73 | 66.86 | 226.95 | 47.75 |

Table 2. Deformation potential constant (E_1), two dimensional elastic constant (C^{2D}), effective mass (m^*), carrier mobility (μ) and relaxation time (τ) at 300 K, 500 K, and 700 K, in the armchair and zigzag directions of the group IV–VI compounds.

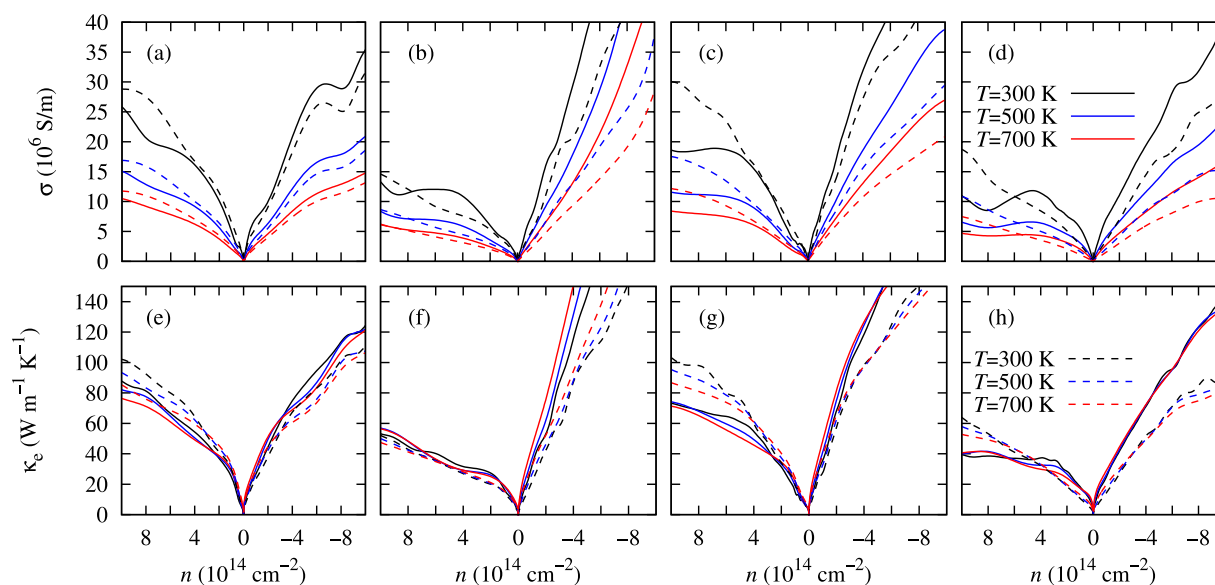


Figure 3. Electrical (σ) and electronic thermal (κ_e) conductivities for the (a,e) SnSe, (b,f) SnS, (c,g) GeSe, and (d,h) GeS along the armchair (solid lines) and zigzag (dashed lines) directions at 300 K, 500 K, and 700 K.

The carrier concentration shows the doping (positive values for p -type doping and negative values for n -type doping). The electrical and thermal conductivities increase by increasing carrier concentration. When the Fermi level occurs in the middle band gap region, the conductivities are increased slowly with respect to the carrier concentration and when it moves down into the valence band (for p -type) or moves up into conduction band (for n -type), the conductivities are increased quickly. GeSe has the highest electrical conductivity of $69.85 \times 10^6 \text{ S/m}$ at $n = -8.9 \times 10^{14} \text{ cm}^{-2}$ in the n -type doping among these compounds. The band gap is higher for the monolayer than bulk (see Table 1). The monolayers have lower electrical conductivity than the bulk due to the increase in the band gaps.

The Seebeck coefficients are calculated as a function of carrier concentration at different temperatures along the armchair and zigzag direction, as shown in Fig. 4. As the temperature decreases, the Seebeck coefficient also increases because of bipolar conduction⁴². The Seebeck coefficients of the two-dimensional monochalcogenides are two times greater than those of the bulk material as shown in the Table 3. This results from, the increase in the band gaps and the density of states near the Fermi level. The GeS has the largest Seebeck coefficient of $2810 \mu \text{VK}^{-1}$ at 300 K because of the large band gap and the flatness in the band structure. The Seebeck coefficient (S) is calculated with the expression,

$$S = \frac{\int_{-\infty}^{\infty} dE g(E)(E - \mu) \left(-\frac{\partial f(E, \mu, T)}{\partial E} \right)}{T \int_{-\infty}^{\infty} dE g(E) \left(\frac{\partial f(E, \mu, T)}{\partial E} \right)}, \quad (4)$$

where E , $g(E)$, $f(E, \mu, T)$, μ , and T are energy, transport function, Fermi function, chemical potential, and temperature, respectively⁴³. The transport function is:

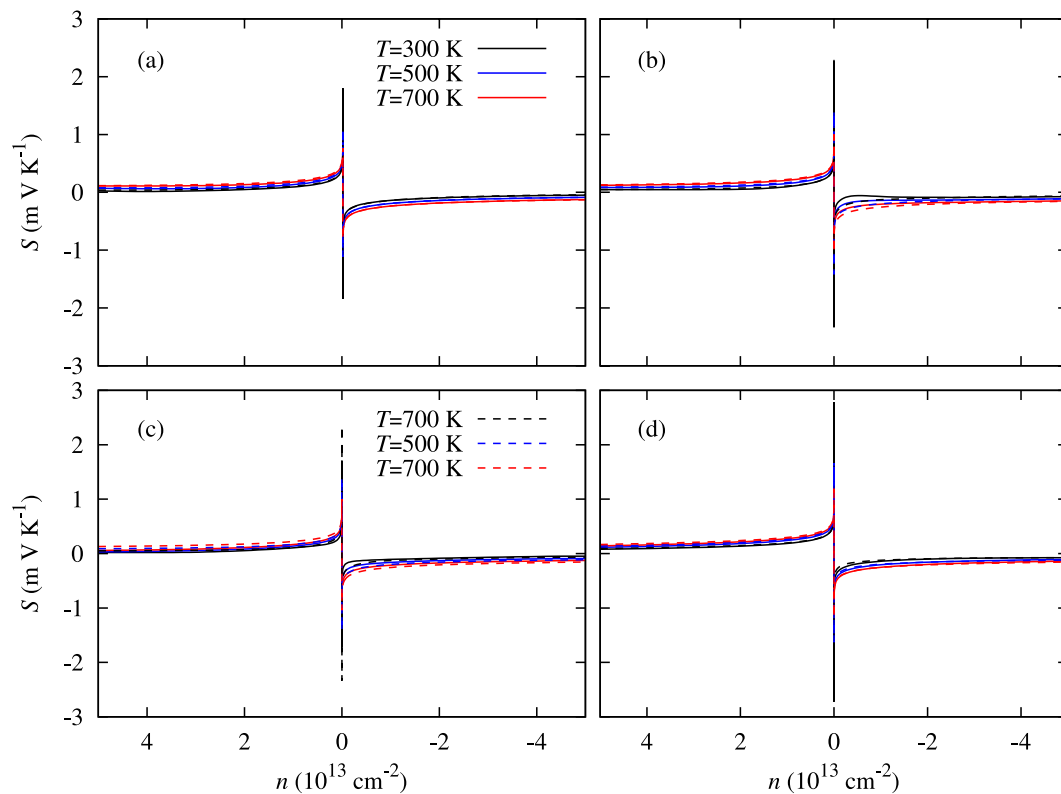


Figure 4. Calculated Seebeck coefficients (S) as a function of the carrier concentration (n) along the armchair (solid lines) and zigzag (dashed lines) directions at 300 K, 500 K, and 700 K for the group IV–VI monolayers (a) SnSe, (b) SnS, (c) GeSe, and (d) GeS.

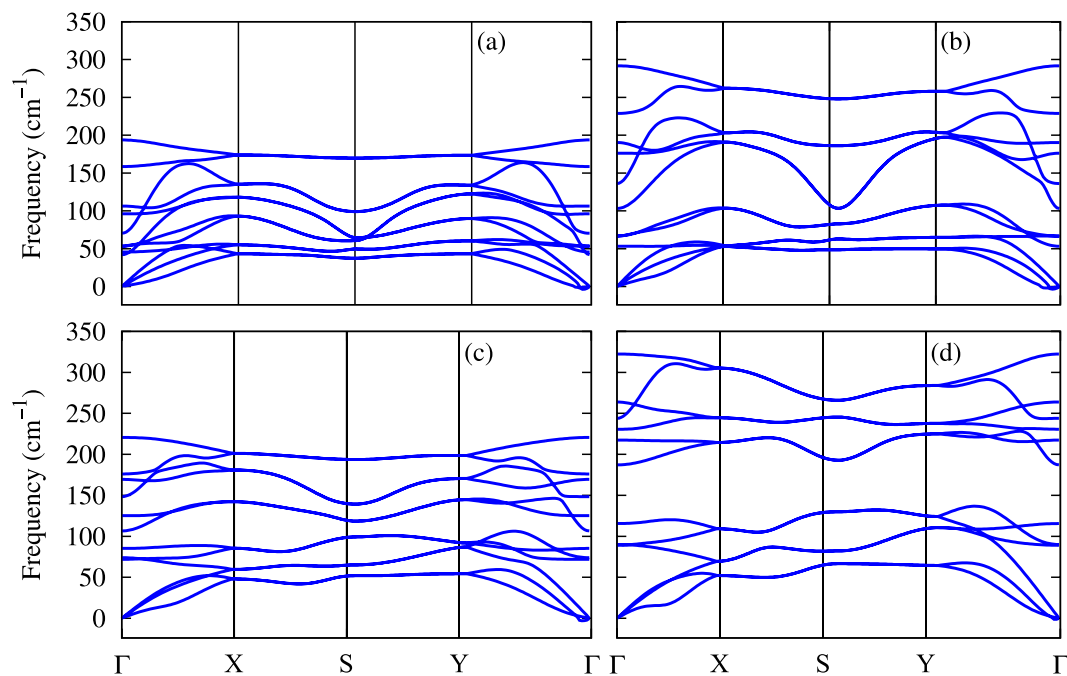


Figure 5. Phonon dispersions along high symmetry k -points for (a) SnSe, (b) SnS, (c) GeSe, and (d) GeS.

| Composition | SnSe | SnS | GeSe | GeS |
|-------------------|------|------|------|------|
| Bulk ¹ | 990 | 1260 | 1240 | 2000 |
| Monolayer | 1750 | 2380 | 1960 | 2810 |

Table 3. The largest values of Seebeck coefficients (S) of bulk and monolayer SnSe, SnS, GeSe, and GeS at 300 K (unit: μVK^{-1}). ¹Ref. 18.

| Material | κ_1 ($\text{Wm}^{-1}\text{K}^{-1}$) | | |
|-------------------|--|--------------------|--------------------|
| | Monolayer | | Bulk |
| | zigzag | armchair | |
| Graphene | 2200 ⁴⁵ | 2200 ⁴⁵ | 2000 ⁴⁸ |
| Phosphorene | 30.1 ⁴⁶ | 13.6 ⁴⁶ | — |
| Bi monolayer | 3.8 ²⁵ | 3.8 ²⁵ | — |
| MoSe ₂ | 70 ⁴⁹ | 70 ⁴⁹ | 40 ⁴⁹ |
| WSe ₂ | 42 ⁴⁹ | 42 ⁴⁹ | 35 ⁴⁹ |
| SnSe | 2.6 | 2.4 | 0.32 ¹⁸ |
| SnS | 4.7 | 4.4 | 0.45 ¹⁸ |
| GeSe | 6.7 | 5.2 | 0.39 ¹⁸ |
| GeS | 10.5 | 7.8 | 0.52 ¹⁸ |

Table 4. Comparison of lattice thermal conductivities κ_l of group IV–VI monolayers with other two-dimensional materials at room temperature.

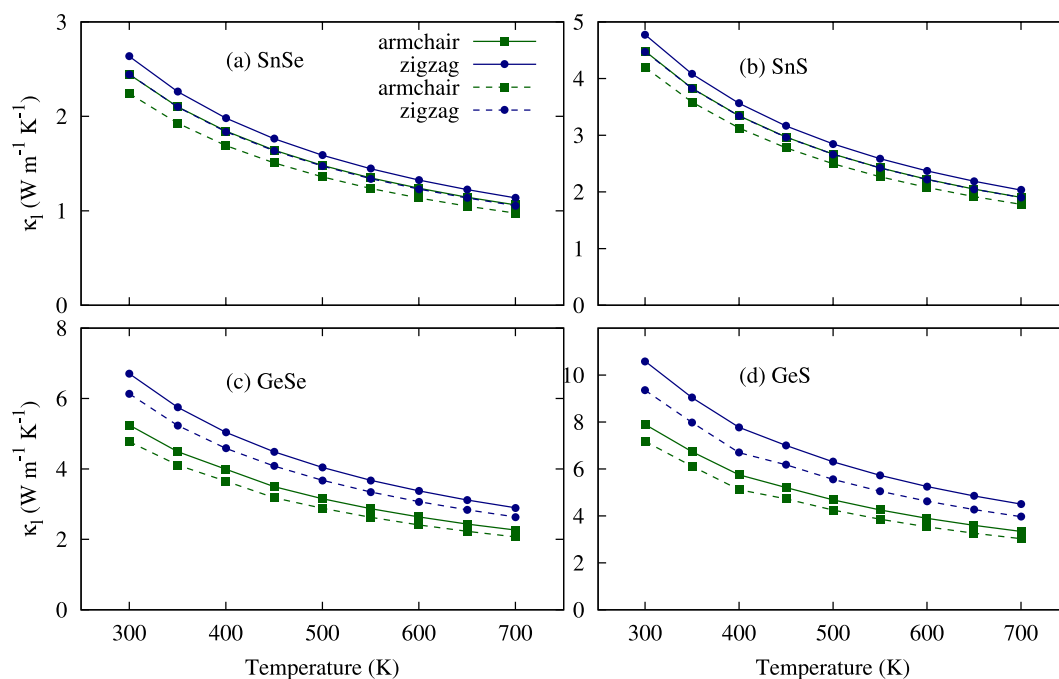


Figure 6. Lattice thermal conductivity (κ_l) for the group IV–VI monolayers are calculated as a function of the temperature using iterative (solid lines) and SMRTA (dashed lines) method.

$$g(E) = N(E)v^2(E)\tau(E), \quad (5)$$

where $N(E)$ is the density of states, $v(E)$ is the Fermi velocity and $\tau(E)$ is the scattering time⁴³. The Seebeck coefficient changes dramatically near the Fermi level because of the term $\frac{\partial f}{\partial E}$ in Eq. 4, which behaves like a Dirac delta function.

Phonon dispersions of SnSe, GeSe, SnS, and GeS were computed to examine the thermal stability using density functional perturbation theory⁴⁴, as shown in Fig. 5. There is no imaginary line in the dispersion curves, which means that these materials are vibrationally stable. There are twelve modes of vibrations: three lower

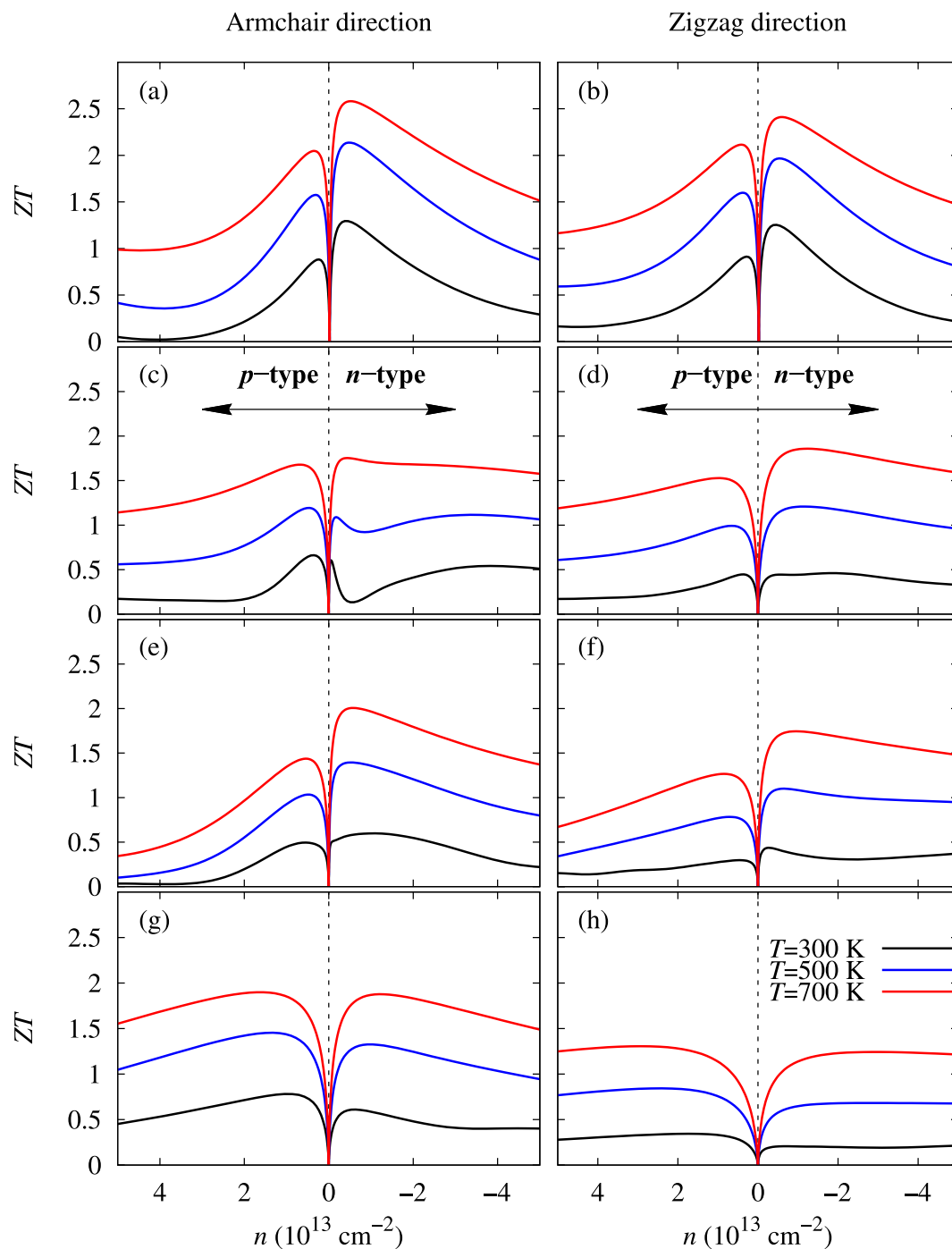


Figure 7. Calculated Figures of merit (ZT) as a function of the carrier concentration (n) for the monolayer of (a,b) SnSe, (c,d) SnS, (e,f) GeSe, and (g,h) GeS along armchair and zigzag directions at temperature 300 K, 500 K, and 700 K.

modes that are acoustic (a transverse acoustic mode, a longitudinal acoustic mode, and a flexural acoustic mode), and the others are optical modes. The flexural acoustic mode is an out-of-plane transverse acoustic mode similar to other two-dimensional materials like graphene, phosphorene, and stanene, quadratic near Γ point^{45–47}. The flexural mode vibrational direction is exactly perpendicular to the plane. It is an important mode in order to understand thermal and mechanical properties of two-dimensional materials.

The lattice conductivities are calculated by solving the Boltzmann transport equation for phonons (BTEP) using the iterative method and the relaxation time approximation (RTA). The iterative method exactly solves the BTEP, while RTA is a good approximation for low conductivity compounds. The results in Fig. 6 show good agreement with recently reported results³⁰. All four of the materials have very low lattice thermal conductivity compared to other two-dimensional materials like graphene, phosphorene, and monolayers of MoSe₂ and WSe₂,

and are comparable to bismuth monolayer as shown in Table 4^{25, 45, 46, 49}. We also found the different lattice thermal conductivity along the armchair and zigzag directions. Because of the heavy masses of Sn and Se, SnSe has the lowest lattice conductivity of $2.44 \text{ Wm}^{-1} \text{ K}^{-1}$ and $2.63 \text{ Wm}^{-1} \text{ K}^{-1}$ at room temperature along the armchair and zigzag directions, respectively.

According to glass dynamical theory, the lattice thermal conductivity is calculated as $\kappa_l = 1/3 C_v l v_s$, where C_v is the heat capacity, l is the mean free path, and v_s is the sound velocity. As the temperature increases, the lattice softens and the stiffness decreases, which reduces the sound velocity and hence the lattice thermal conductivity⁵⁰. This trend is shown in Fig. 6.

Finally, using the Seebeck coefficient and the electrical and thermal conductivities, we calculated ZT as a function of the carrier concentration along the armchair and zigzag directions at 300 K, 500 K, and 700 K, as shown in Fig. 7. These monolayers had very high ZT . SnSe had the highest ZT of 2.63 along the armchair direction at 700 K because of the high electrical conductivity and Seebeck coefficient and the low lattice thermal conductivity. In the case SnS, a high ZT of 1.88 is predicted along the zigzag direction.

Conclusion. We analyzed the structural, electronic, thermoelectric, and phonon-transport properties of the two-dimensional monochalcogenide compounds SnSe, SnS, GeSe, and GeS using density functional theory combined with Boltzmann transport theory for electrons and phonons. These compounds are energetically and vibrationally stable, and SnSe, SnS, and GeS have indirect band gaps while GeSe has a direct band gap. The Seebeck coefficients of these two-dimensional materials are two times larger than those of their bulk structures, and two-dimensional GeS has the largest Seebeck coefficient of $2810 \mu \text{ V K}^{-1}$ at room temperature. These monolayer materials have very low lattice thermal conductivities in comparison to other two-dimensional materials. ZT of SnSe, GeSe and GeS along the armchair direction was 2.63, 1.99, and 1.85, respectively, while that of ZT of SnS along the zigzag direction was 1.88. These ZT values are higher than those of their bulk analogs. Hence, the materials are very promising for thermoelectric applications.

Methods

Our calculations are based on density functional theory combined with Boltzmann transport theory and were performed using the Vienna Ab initio Simulation Package (VASP) and the Boltztrap code^{51–53}. The generalized gradient approximation proposed by Perdew–Burke–Ernzerhof was chosen as an electronic exchange correlation functional⁵⁴. The vdW-DF scheme is used to include the van der Waals interaction⁵⁵. A Monkhorst mesh of $10 \times 10 \times 1$ k -points is used for lattice optimization and 450 eV is used as a plane wave cutoff energy. Structures are optimized until the Hellmann–Feynman force on each atom is less than 0.001 eV/\AA . A vacuum region of 15 \AA in the z -direction is produced to avoid the interaction between periodic images.

Thermoelectric properties were computed by solving the Boltzmann transport equation under a constant relaxation time (τ) and a rigid band approximation performed in the Boltztrap code⁵³. We used a very dense k -point mesh of $60 \times 60 \times 1$ to obtain a convergent density of states. The Seebeck coefficient $S(T, n)$, electrical (σ/τ) and electronic thermal (κ_e/τ) conductivities divided by the relaxation time were calculated. Boltztrap code used Wiedemann–Franz law to calculate electronic thermal conductivity from electrical conductivity.

To calculate the lattice thermal conductivity (κ_l), we used the ShengBTE code⁵⁶. The second-order (harmonic) and the third-order (anharmonic) interatomic force constants (IFCs) are required to calculate lattice thermal conductivity. In order to calculate the second-order IFCs, we used the Phonopy code with a supercell of $5 \times 5 \times 1$ and a k -mesh of $10 \times 10 \times 1$. For the third-order IFCs, a supercell of $4 \times 4 \times 1$ was used with the of interactions up to the 15th nearest neighbors^{57–59}.

References

- Snyder, G. J. & Toberer, E. S. Complex thermoelectric materials. *Nat. Mater.* **7**, 105–114 (2008).
- Sun, B. Z., Ma, Z., He, C. & Wu, K. Anisotropic thermoelectric properties of layered compounds in SnX_2 ($X = \text{S, Se}$): a promising thermoelectric material. *Phys. Chem. Chem. Phys.* **17**, 29844–29853 (2015).
- DiSalvo, F. J. Thermoelectric cooling and power generation. *Sci.* **285**, 703–706 (1999).
- Ding, G., Gao, G. Y. & Yao, K. L. Examining the thermal conductivity of the half-Heusler alloy TiNiSn by first-principles calculations. *J. Phys. D: Appl. Phys.* **48**, 235302 (2015).
- Ong, K. P., Singh, D. J. & Wu, P. Analysis of the thermoelectric properties of n -type ZnO . *Phys. Rev. B* **83**, 115110 (2011).
- Ohta, H. *et al.* Giant thermoelectric Seebeck coefficient of a two-dimensional electron gas in SrTiO_3 . *Nat. Mater.* **6**, 129–134 (2007).
- Kishimoto, K. & Koyanagi, T. Preparation of sintered degenerate n -type PbTe with a small grain size and its thermoelectric properties. *J. Appl. Phys.* **92**, 2544 (2002).
- Ibrahiman, A. M. & Thompson, D. A. Thermoelectric properties of BiSb alloys. *Mater. Chem. Phys.* **12**, 29–36 (1985).
- Snyder, G. J., Christensen, M., Nishibori, E., Caillat, T. & Iversen, B. B. Disordered zinc in Zn_4Sb_3 with phonon-glass and electron-crystal thermoelectric properties. *Nat. Mater.* **3**, 458–463 (2004).
- Tang, X., Chen, L., Goto, T. & Hirai, T. Effects of Ce filling fraction and Fe content on the thermoelectric properties of Co-rich $\text{Ce}_x\text{Co}_{4-x}\text{Sb}_{12}$. *J. Mater. Res.* **16**, 837–843 (2001).
- Sales, B. C., Mandrus, D., Chakoumakos, B. C., Keppens, V. & Thompson, J. R. Filled skutterudite antimonides: Electron crystals and phonon glasses. *Phys. Rev. B* **56**, 15081–15089 (1997).
- Nolas, G. S., Kaeser, M., Littleton, R. T. & Tritt, T. M. High figure of merit in partially filled ytterbium skutterudite materials. *Appl. Phys. Lett.* **77**, 1855–1857 (2000).
- Nolas, G. S., Cohn, J. L., Slack, G. A. & Schujman, S. B. Semiconducting Ge clathrates: Promising candidates for thermoelectric applications. *Appl. Phys. Lett.* **73**, 178–180 (1998).
- Sekimoto, T., Kurosaki, K., Muta, H. & Yamanaka, S. High-Thermoelectric figure of merit realized in p -type half-Heusler compounds: $\text{ZrCoSn}_x\text{Sb}_{1-x}$. *Jap. J. Appl. Phys.* **46**, L673–L675 (2007).
- Singh, I. I. & Mazin, D. J. Calculated thermoelectric properties of La-filled skutterudites. *Phys. Rev. B* **56**, R1650–R1653 (1997).
- Sootsman, J. R., Chung, D. Y. & Kanatzidis, M. G. New and old concepts in thermoelectric materials. *Ang. Chem. Inter. Edit.* **48**, 8616–8639 (2009).
- Zhao, L. D. *et al.* Ultralow thermal conductivity and high thermoelectric figure of merit in SnSe crystals. *Nature* **508**, 373–377 (2014).

18. Ding, G., Gao, G. & Yao, K. High-efficient thermoelectric materials: The case of orthorhombic IV–VI compounds. *Sci. Rep.* **5**, 9567 (2015).
19. Dresselhaus, M. S. *et al.* New directions for low-dimensional thermoelectric materials. *Adv. Mater.* **38**, 1043–1053 (2007).
20. Szczech, J. R., Higgins, J. M. & Jin, S. Enhancement of the thermoelectric properties in nanoscale and nanostructured materials. *J. Mater. Chem.* **21**, 4037 (2011).
21. Hicks, L. D. & Dresselhaus, M. S. Thermoelectric figure of merit of a one-dimensional conductor. *Phys. Rev. B* **47**, 16631–16634 (1993).
22. Samad, A., Noor-A-Alam, M. & Shin, Y.-H. First principles study of a SnS₂/graphene heterostructure: a promising anode material for rechargeable Na ion batteries. *J. Mater. Chem. A* **4**, 14316–14323 (2016).
23. Hicks, L. D. & Dresselhaus, M. S. Effect of quantum-well structures on the thermoelectric figure of merit. *Phys. Rev. B* **47**, 12727–12731 (1993).
24. Fei, R. *et al.* Enhanced thermoelectric efficiency via orthogonal electrical and thermal conductances in phosphorene. *Nano Lett.* **14**, 6393–6399 (2014).
25. Cheng, L. *et al.* Thermoelectric properties of a monolayer bismuth. *J. Phys. Chem. C* **118**, 904–910 (2014).
26. Li, L. *et al.* Single-layer single-crystalline sncs nanosheets. *J. Am. Chem. Soc.* **135**, 1213–1216 (2013).
27. Xia, J. *et al.* Physical vapor deposition synthesis of two-dimensional orthorhombic SnS flakes with strong angle/temperature-dependent Raman responses. *Nanoscale* **8**, 2063–2070 (2016).
28. Li, X. *et al.* Controlled vapor phase growth of single crystalline, two-dimensional GaSe crystals with high photoresponse. *Sci. Rep.* **4**, 5497 (2014).
29. Zhang, S. *et al.* Two-dimensional GeS with tunable electronic properties via external electric field and strain. *Nanotechnology* **27**, 274001 (2016).
30. Qin, G. *et al.* Diverse anisotropy of phonon transport in two-dimensional group IV–VI compounds: A comparative study. *Nanoscale* **8**, 11306–11319 (2016).
31. Zhao, L.-D., Tan, G., Hao, S., He, J., Pei, Y., Chi, H., Wang, H., Gong, S., Xu, H., Dravid, V. P., Uher, C., Snyder, G. J., Wolverton, C. & Kanatzidis, M. G. Ultrahigh power factor and thermoelectric performance in hole-doped single-crystal SnSe. *Science* **351**, 141–144 (2015).
32. Zhao, L.-D., Chang, C., Tan, G. & Kanatzidis, M. G. SnSe: a remarkable new thermoelectric material. *Energy Environ. Sci.* **9**, 3044–3060 (2016).
33. Wang, F. Q., Zhang, S., Yu, J. & Wang, Q. Thermoelectric properties of single-layered SnSe sheet. *Nanoscale* **7**, 15962–15970 (2015).
34. Singh, A. K. & Hennig, R. G. Computational prediction of two-dimensional group-IV mono-chalcogenides. *Appl. Phys. Lett.* **105**, 042103 (2014).
35. Fei, R., Li, W., Li, J. & Yang, L. Giant piezoelectricity of monolayer group IV monochalcogenides: SnSe, SnS, GeSe, and GeS. *Appl. Phys. Lett.* **107**, 173104 (2015).
36. Lv, H. Y., Lu, W. J., Shao, D. F., Lu, H. Y. & Sun, Y. P. Strain-induced enhancement in the thermoelectric performance of a ZrS₂ monolayer. *J. Mater. Chem. C* **4**, 4538–4545 (2016).
37. Jin, Z., Liao, Q., Fang, H., Liu, Z., Liu, W., Ding, Z., Luo, T. & Yang, N. A Revisit to High Thermoelectric Performance of Single-layer MoS₂. *Sci. Rep.* **5**, 18342 (2015).
38. Zhang, L.-C., Qin, G., Fang, W.-Z., Cui, H.-J., Zheng, Q.-R., Yan, Q.-B. & Su, G. Tinselenidene: a Two-dimensional Auxetic Material with Ultralow Lattice Thermal Conductivity and Ultrahigh Hole Mobility. *Sci. Rep.* **6**, 19830 (2016).
39. Cai, Y., Zhang, G. & Zhang, Y.-W. Polarity-Reversed Robust Carrier Mobility in Monolayer MoS₂ Nanoribbons. *J. Am. Chem. Soc.* **136**, 6269–6275 (2014).
40. Bardeen, J. & Shockley, W. Deformation Potentials and Mobilities in Non-Polar Crystals. *Phys. Rev.* **80**, 72–80 (1950).
41. Huang, L., Wu, F. & Li, J. Structural anisotropy results in strain-tunable electronic and optical properties in monolayer GeX and SnX (X = S, Se, Te). *J. Chem. Phys.* **144**, 114708 (2016).
42. Bahk, J.-H. & Shakouri, A. Enhancing the thermoelectric figure of merit through the reduction of bipolar thermal conductivity with heterostructure barriers. *Appl. Phys. Lett.* **105**, 052106 (2014).
43. Parker, D. & Singh, D. J. Thermoelectric properties of AgGaTe₂ and related chalcopyrite structure materials. *Phys. Rev. B* **85**, 125209 (2012).
44. Baroni, S., de Gironcoli, S., Dal Corso, A. & Giannozzi, P. Phonons and related crystal properties from density-functional perturbation theory. *Rev. Mod. Phys.* **73**, 515–562 (2001).
45. Kong, B. D., Paul, S., Nardelli, M. B. & Kim, K. W. First-principles analysis of lattice thermal conductivity in monolayer and bilayer graphene. *Phys. Rev. B* **80**, 033406 (2009).
46. Qin, G. *et al.* Anisotropic intrinsic lattice thermal conductivity of phosphorene from first principles. *Phys. Chem. Chem. Phys.* **17**, 4854–4858 (2015).
47. Peng, B. *et al.* Low lattice thermal conductivity of stanene. *Sci. Rep.* **6**, 20225 (2016).
48. Nika, D. L., Ghosh, S., Pokatilov, E. P. & Balandin, A. A. Lattice thermal conductivity of graphene flakes: Comparison with bulk graphite. *Appl. Phys. Lett.* **94**, 203103 (2009).
49. Kumar, S. & Schwingenschlogl, U. Thermoelectric response of bulk and monolayer MoSe₂ and WSe₂. *Chem. Mater.* **27**, 1278–1284 (2015).
50. Dugdale, J. S. & MacDonald, D. K. C. Lattice thermal conductivity. *Phys. Rev.* **98**, 1751–1752 (1955).
51. Kresse, G. & Furthmüller, J. Efficient iterative schemes for *ab initio* total-energy calculations using a plane-wave basis set. *Phys. Rev. B* **54**, 11169–11186 (1996).
52. Kresse, G. & Joubert, D. From ultrasoft pseudopotentials to the projector augmented-wave method. *Phys. Rev. B* **59**, 1758–1775 (1999).
53. Madsen, G. K. & Singh, D. J. BoltzTraP. A code for calculating band-structure dependent quantities. *Comp. Phys. Commun.* **175**, 67–71 (2006).
54. Perdew, J. P., Burke, K. & Ernzerhof, M. Generalized gradient approximation made simple. *Phys. Rev. Lett.* **77**, 3865–3868 (1996).
55. Klimeš, J., Jev, Bowler, D. R. & Michaelides, A. Van der Waals density functionals applied to solids. *Phys. Rev. B* **83**, 195131 (2011).
56. Li, W., Carrete, J., A. Katcho, N. & Mingo, N. ShengBTE: A solver of the Boltzmann transport equation for phonons. *Comp. Phys. Commun.* **185**, 1747–1758 (2014).
57. Togo, A., Oba, F. & Tanaka, I. First-principles calculations of the ferroelastic transition between rutile-type and CaCl₂-type SiO₂ at high pressures. *Phys. Rev. B* **78**, 134106 (2008).
58. Li, W., Lindsay, L., Broido, D. A., Stewart, D. A. & Mingo, N. Thermal conductivity of bulk and nanowire Mg₂Si_xSn_{1-x} alloys from first principles. *Phys. Rev. B* **86**, 174307 (2012).
59. Li, W. *et al.* Thermal conductivity of diamond nanowires from first principles. *Phys. Rev. B* **85**, 195436 (2012).

Acknowledgements

This work was supported by the Basic Science Research Program (NRF-2014R1A2A1A11050893), Nano-Material Technology Development Program (NRF-2014M3A7B4049367), Basic Research Laboratory (NRF-

2014R1A4A1071686), and Priority Research Center Program (2009-0093818) through the National Research Foundation of Korea, which is funded by the Ministry of Science, ICT & Future Planning.

Author Contributions

A.S. performed the calculations, and analyzed the results. All authors reviewed the manuscript.

Additional Information

Supplementary information accompanies this paper at doi:[10.1038/s41598-017-00598-7](https://doi.org/10.1038/s41598-017-00598-7)

Competing Interests: The authors declare that they have no competing interests.

Publisher's note: Springer Nature remains neutral with regard to jurisdictional claims in published maps and institutional affiliations.



This work is licensed under a Creative Commons Attribution 4.0 International License. The images or other third party material in this article are included in the article's Creative Commons license, unless indicated otherwise in the credit line; if the material is not included under the Creative Commons license, users will need to obtain permission from the license holder to reproduce the material. To view a copy of this license, visit <http://creativecommons.org/licenses/by/4.0/>

© The Author(s) 2017